CrossMark

HEPATOBILIARY-PANCREAS

Gadoxetate-enhanced MR imaging and compartmental modelling to assess hepatocyte bidirectional transport function in rats with advanced liver fibrosis

Céline Giraudeau[1] · Benjamin Leporq[1] · Sabrina Doblas[1] · Matthieu Lagadec[1,2] ·
Catherine M. Pastor[1,3] · Jean-Luc Daire[1,2] · Bernard E. Van Beers[1,2]

Abstract

Objectives Changes in the expression of hepatocyte membrane transporters in advanced fibrosis decrease the hepatic transport function of organic anions. The aim of our study was to assess if these changes can be evaluated with pharmacokinetic analysis of the hepatobiliary transport of the MR contrast agent gadoxetate.

Methods Dynamic gadoxetate-enhanced MRI was performed in 17 rats with advanced fibrosis and 8 normal rats. After deconvolution, hepatocyte three-compartmental analysis was performed to calculate the hepatocyte influx, biliary efflux and sinusoidal backflux rates. The expression of Oatp1a1, Mrp2 and Mrp3 organic anion membrane transporters was assessed with reverse transcription polymerase chain reaction.

Results In the rats with advanced fibrosis, the influx and efflux rates of gadoxetate decreased and the backflux rate increased significantly (p = 0.003, 0.041 and 0.010, respectively). Significant correlations were found between influx and Oatp1a1 expression (r = 0.78, p < 0.001), biliary efflux and Mrp2 (r = 0.50, p = 0.016) and sinusoidal backflux and Mrp3 (r = 0.61, p = 0.002).

Conclusion These results show that changes in the bidirectional organic anion hepatocyte transport function in rats with advanced liver fibrosis can be assessed with compartmental analysis of gadoxetate-enhanced MRI.

Key Points
• *Expression of hepatocyte transporters is modified in rats with advanced liver fibrosis.*
• *Kinetic parameters at gadoxetate-enhanced MRI are correlated with hepatocyte transporter expression.*
• *Hepatocyte transport function can be assessed with compartmental analysis of gadoxetate-enhanced MRI.*
• *Compartmental analysis of gadoxetate-enhanced MRI might provide biomarkers in advanced liver fibrosis.*

Introduction

Assessing liver function, and more particularly transport function and biliary elimination, is decisive in determining therapeutic effects and toxicity of drugs using this elimination pathway [1]. Furthermore, assessment of liver function is critical in determining the prognosis in patients with advanced chronic liver diseases or undergoing extensive liver surgery [2]. Among hepatocyte transport systems, the organic anion transport system allows elimination of a wide variety of endogenous substances and xenobiotics [3, 4].

Organic anions pass through the sinusoidal membrane of the hepatocytes using organic anion transporting polypeptides (Oatp1a1 in rats). The organic anions are excreted into the bile through the multidrug resistance protein transporters Mrp2. Sinusoidal backflux occurs through Mrp3 and through the bidirectional Oatp1a1 transporters [5, 6]. The expression of hepatocyte membrane transporters is modified in liver

✉ Céline Giraudeau
  giraudeau.celine@hotmail.fr

1 Laboratory of Imaging Biomarkers, UMR1149 Inserm, University Paris Diderot, Sorbonne Paris Cité, Hôpital Beaujon, 100 boulevard du général Leclerc, 92110 Clichy, France

2 Department of Radiology, Beaujon University Hospital Paris Nord, Clichy, France

3 Département d'imagerie et des sciences de l'information médicale, Hôpitaux Universitaires de Genève, Geneva, Switzerland

diseases. In liver fibrosis and cirrhosis, decreases in Oatp1a1 and Mrp2 as well as an increase in Mrp3 expression are observed [4].

The hepatocyte transport of organic anions can be approached by compartmental or non-compartmental analysis of contrast agent kinetics at ^{99m}Tc-iminodiacetic (IDA) scintigraphy, [7, 8]. It has been reported that the hepatocyte influx (k_{21}), efflux (k_{32}) and backflux (k_{12}) rates can be assessed with compartmental analysis at ^{99m}Tc-IDA scintigraphy [7–9]. However, this nuclear medicine method is limited by low spatial and temporal resolution.

More recently, MRI enhanced with hepatobiliary contrast agents has been proposed to assess liver function. These hepatobiliary contrast agents include gadoxetic and gadobenic acid which use similar hepatocyte membrane transporters but differ in their hepatic uptake, which is 50 % for gadoxetic acid and 5 % for gadobenic acid [5]. Because of its high hepatocyte uptake, gadoxetic acid has been more extensively studied than gadobenic acid for liver function assessment [10–15]. However, pharmacokinetic assessment with gadoxetate-enhanced MRI has been limited to hepatocyte influx only, without analysis of the efflux and backflux functions.

The aim of this study was to investigate the feasibility of studying bidirectional changes in the organic anion transport function in liver fibrosis with compartmental analysis of gadoxetate-enhanced MRI.

## Material and methods

Animal model and MRI study

All experimental procedures were approved by the animal ethics committee of our institution. The study was carried out on MRI data acquired in a previously reported study in which the animal model and MRI acquisitions were described [14]. Briefly, 8-week-old male Wistar rats (280–330 g) were injected intraperitoneally twice a week with carbon tetrachloride (CCl$_4$, 0.1 ml/100 g diluted to 50 % in olive oil) over 8 (n = 9 rats) or 12 weeks (n = last 12 rats) to induce advanced liver fibrosis. Indeed, in the CCl4-induced rat fibrosis model, it is known that fibrosis develops progressively with severe bridging fibrosis (F3) after 5–7 weeks and cirrhosis (F4) after 8–9 weeks after administration. After 10–20 weeks, micronodular cirrhosis, portal hypertension and ascites appear progressively. Timing for those lesions will largely vary depending on species, strain, dose, route and frequency of administration [16]. Four rats died during fibrosis induction. MRI was performed in 17 rats 2 days after the last CCl$_4$ injection. MRI was also performed in eight normal rats used as controls.

The rats were anaesthetised with isoflurane inhalation and a catheter was placed in the tail vein. Imaging was carried out with a 7 T PharmaScan small animal scanner (Bruker, Ettlingen, Germany) and a transmitter/receiver birdcage coil. The rats were placed in the supine position. Respiratory-triggered T$_2$-weighted anatomical images of the liver were acquired with a RARE sequence (effective TE = 23 ms, TR = 3,000 ms, RARE factor 4, 0.5× 0.5 mm^2 in-plane resolution). Dynamic gadoxetate-enhanced MRI was performed with a FLASH sequence (TE = 2.16 ms, TR = 20.5 ms, flip angle = 25°, partial Fourier 6/8, 80 × 80 pixels, 0.75 × 0.75 mm^2 in-plane resolution, two transverse 2-mm thick slices, acquisition time = 1.23 s and 3,500 repetitions, total acquisition time 72 min). Two saturation bands were placed above and beneath the liver sections. After 1 min image acquisition, the rats were manually injected with 1 ml/kg with a 1:10 dilution of gadoxetate (Primovist®, Bayer Healthcare, Berlin, Germany) through the implanted catheter. The two transverse slices were positioned in the upper and lower halves of the liver.

Image processing and deconvolution operation

Only the lowest liver section, passing through the right hepatic lobe and the portal vein, was used for image analysis. To obtain images without interpolation or filtering, image reconstruction from raw data was performed with Matlab (Mathworks, Natick, MA, USA) and their complex components were averaged over four acquisitions to reduce the noise. Regions of interest (ROIs) were put in the liver parenchyma and in the portal vein by an observer (C.G. with 4 years of experience in small-animal MRI) who was blinded to the histopathological results. The ROIs in the portal vein covered the whole venous section but avoided the vessel borders. The ROIs were adjusted manually as needed. The ROIs in the right liver lobe covered a large area of parenchyma devoid of large vessels (Fig. 1).
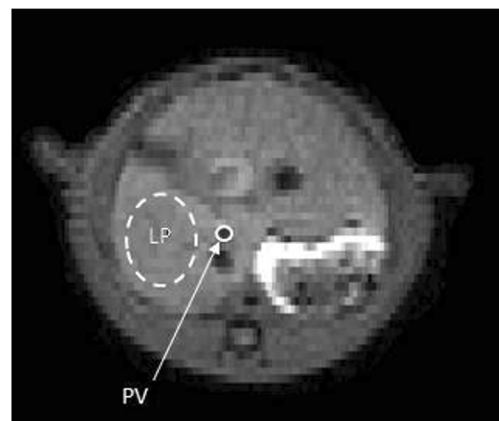
Fig. 1 Transverse MR image of a rat as acquired during the dynamic study showing the regions of interest (ROIs) in right liver parenchyma (LP) and portal vein (PV)

Relative concentration curves [10, 17] in the ROIs were calculated as:

$$C(t,\rho) = \ln\left(\frac{S(t,\rho)}{S_0(\rho)}\right) \tag{1}$$

where $C(t,\rho)$ is the relative tracer concentration at time t in pixel ρ, $S_0(\rho)$ is the mean image intensity in voxel ρ obtained from the unenhanced images, and $S(t,\rho)$ is the measured image intensity at time t.
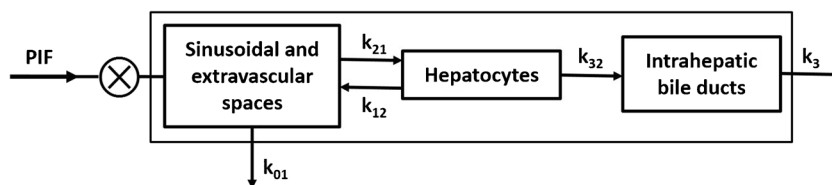
As gadoxetate uptake in hepatocytes is affected by hepatic perfusion [10], deconvolution was performed. The response function of the liver can be mathematically expressed as the convolution between the tissue impulse response h(t) and the vascular input function x(t):

$$y(t) = h(t) \otimes x(t) \tag{2}$$

where $\otimes$ denotes the convolution operator, y(t) the parenchymal enhancement-over-time curve or hepatic response function, x(t) the portal venous enhancement-over-time curve or portal venous input function and h(t) the liver impulse response. Deconvolution was performed with the truncated singular value decomposition method [10] using truncation of singular values below 10 % of the maximum value.

Compartmental analysis

Least-square fittings were carried out with Matlab routines. To express h(t) with kinetic indices k_{ij}, we modelled the liver with a three-compartment hepatocyte model composed of sinusoidal and extravascular spaces, hepatocytes and intrahepatic bile ducts [7]. The sinusoidal and extravascular spaces were grouped together because the sinusoidal endothelium contains fenestrae of 100–200 nm in the normal liver, allowing for free access of solutes and macromolecules into the extravascular space [18]. Gadoxetate exchange between these compartments is governed by the hepatocyte influx rate (k_{21} in min^{-1}), the biliary efflux (k_{32} in min^{-1}) and the sinusoidal backflux (k_{12} in min^{-1}). Moreover, venous and bile outflows occur at rates of k_{01} and k_3, respectively (Fig. 2).

The liver impulse response h(t) can be decomposed into two impulse functions:

$$h(t) = h_e(t) + h_p(t) \tag{3}$$

where $h_e(t)$ and $h_p(t)$ represent the gadoxetate fractions in the extracellular and cellular compartment respectively. According to van Beers et al. [19]:

$$h_e(t) = e^{-k_{01}t} = e^{-\frac{t}{MTT}} \tag{4}$$

where MTT is the extracellular mean transit time.

The model was simplified by assuming that $h_e(t)$ could be neglected ($h_e(t) \approx h(t)$) because MTT is short relative to the mean residence time of the contrast agent within the liver. Indeed, reported MTTs of small-molecular weight agents (gadoterate in rabbits) were < 10 s, whereas hepatic half-life times of small-molecular weight agents (mebrofenin in rats) were around 10 min [19, 20].

With the three-compartmental model, h(t) can be expressed as (see Appendix):

$$h(t) = k_{21} - \frac{k_{21}k_{32}}{k_{32} + k_{12} - k_3} e^{-(k_{32}+k_{12})t}$$
$$+ \frac{k_{21}k_{32}}{k_{32} + k_{12} - k_3} e^{-k_3 t} \tag{5}$$

By assuming $k_3 = k_{32}$ [7, 8]:

$$h(t) = k_{21} - \frac{k_{21}k_{32}}{k_{12}} e^{-(k_{32}+k_{12})t} + \frac{k_{21}k_{32}}{k_{12}} e^{-k_{32}t} \tag{6}$$

To take into account the relative volume difference between the hepatocytes and the bile ducts within the hepatic non-vascular/extravascular pool, volume correction factors of 0.99 and 0.01, respectively, were added [21], so that the impulse response h(t) was expressed as:

$$h(t) = 0.99k_{21}\left(1 - \frac{k_{21}k_{32}}{k_{12}}\right)e^{-(k_{32}+k_{12})t}$$
$$+ 0.01\frac{k_{21}k_{32}}{k_{12}} e^{-k_{32}t} \tag{7}$$

The influx k_{21}, the efflux k_{32} and the backflux k_{12} rates were measured by fitting the deconvoluted curve with the

Fig. 2 The hepatocyte three-compartment model representing gadoxetate exchanges between sinusoidal and extravascular spaces, hepatocytes and intrahepatic bile ducts. The hepatocyte influx rate (k_{21}), the biliary efflux rate (k_{32}) and the sinusoidal backflux rate (k_{12}) are fractional rates representing the fraction of gadoxetate that is exchanged between the compartments per minute, PIF is the portal venous input flow and k_{01} and k_3 the venous and bile outflows, respectively

above model. Lower and upper bounds were included in the fitting procedure to keep the rates physiologically relevant (for k_{21} lower and upper bounds were 0.01 and 5 min^{-1} respectively, and for k_{32} and k_{12} lower and upper bounds were 0.0001 and 2 min^{-1}, respectively) [7].

Histology and transporter analysis

After imaging, the rats were sacrificed by intraperitoneal injection of pentobarbital and the livers were resected. The right liver lobe was fixed in formaldehyde and embedded in paraffin. Slices were stained with Sirius red and fibrosis was staged according to the METAVIR score from F0 to F4 by a pathologist (VP) with 23 years' experience in liver pathology [22]. Expressions of Oatp1a1, Mrp2 and Mrp3 transporters were assessed on additional liver samples collected for reverse transcription polymerase chain reaction (RT-PCR), as described previously [14]. The expression of the transporters was compared with that of beta-glucuronidase to normalize the expression levels of the target genes (expressed in %).

Statistical analysis and correlations

Results are expressed as mean ± standard deviation. Comparisons between control rats and rats with advanced fibrosis were performed with two-sample Student's tests. Pearson correlation coefficients were calculated to assess the relationship between the kinetic rates and the expression of the corresponding hepatocyte transporters (k_{21} and Oatp1a1, k_{32} and Mrp2, and k_{12} and Mpr3, respectively).

The analysis was performed in 15 rats with advanced liver fibrosis and eight normal rats. The results of two additional rats with advanced liver fibrosis were excluded from the analysis because RT-PCR yielded very high, aberrant Mrp3 values (one greater order of magnitude than that of the other fibrotic rats). P-values ≤ 0.05 were considered statistically significant.
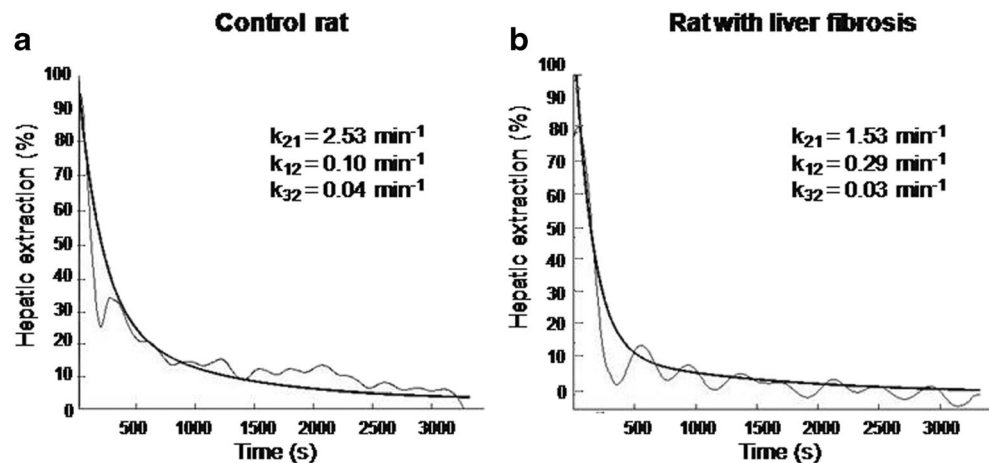
Results

Regarding the METAVIR scores, the livers of the control animals (n = 8) were F0, whereas those of the CCl$_4$-injected animals were F3 (n = 2) or F4 (n = 13). The influx and efflux rates k_{21} and k_{32} decreased significantly in rats with advanced liver fibrosis relative to control rats (1.58 ± 0.76 min^{-1} vs. 2.62 ± 0.52 min^{-1}, p = 0.003 and 0.03 ± 0.01 min^{-1} vs. 0.04 ± 0.01 min^{-1}, p = 0.041, respectively), whereas the backflux rate k_{12} increased significantly (0.23 ± 0.10 min^{-1} vs. 0.11 ± 0.08 min^{-1}, p = 0.010) (Figs. 3 and 4). In parallel, RT-PCR showed significant decreases in Oatp1a1 (2.40 ± 1.92 % vs. 5.26 ± 1.95 %, p = 0.007) and Mrp2 transporter expression (2.79 ± 2.57 % vs. 6.83 ± 1.65 %, p < 0.001) and a significant increase in Mrp3 expression (0.24 ± 0.12 % vs. 0.05 ± 0.02 %, p < 0.001) in rats with advanced liver fibrosis versus control rats.
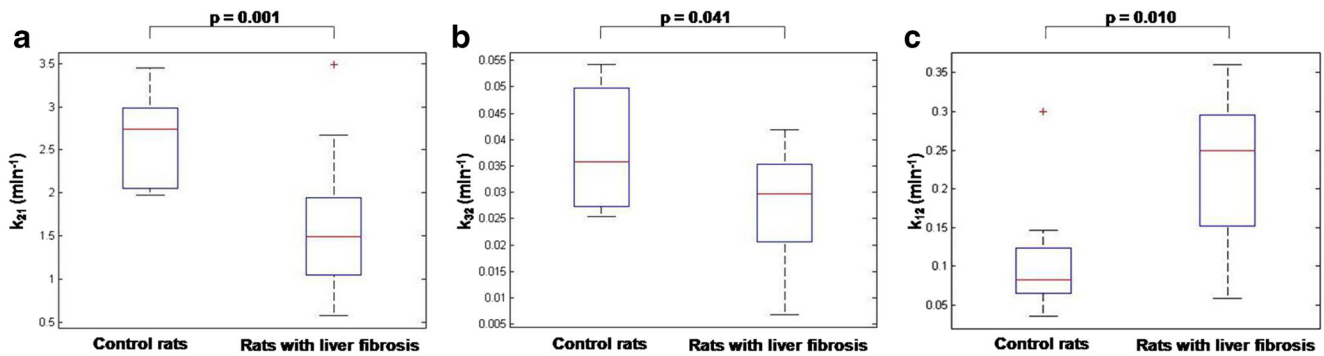
Significant correlations were found between k_{21} and Oatp1a1 expression (r = 0.78, p < 0.001), k_{32} and Mrp2 (r = 0.50, p = 0.016), and k_{12} and Mrp3 (r = 0.61, p = 0.002) (Fig. 5).

Discussion

In our rat model of advanced liver fibrosis, we observed complex changes in the hepatocyte transport of the organic anion gadoxetate. There was not only a significant decrease in hepatocyte influx (k_{21}), but also in biliary efflux (k_{32}), and a significant increase in sinusoidal backflux (k_{12}). These kinetic changes can be explained by changes in the expression of the different hepatocyte membrane transporters, as shown by the significant correlations between the kinetic rates and the expression of the corresponding transporters. Indeed, in liver fibrosis, we observed, as previously reported, not only a decrease in Oatp1a, a bidirectional transporter at the sinusoidal membrane of the hepatocyte, but also a decrease in the biliary

Fig. 3 Deconvoluted curves of a control rat (**A**) and a rat with advanced liver fibrosis (**B**, *light grey*: deconvoluted curve, *bold*: fitted curve). Influx (k_{21}) and efflux (k_{32}) rates are decreased in the rat with liver fibrosis versus the control rat, whereas the backflux rate (k_{12}) is increased

Control rat
$k_{21} = 2.53$ min^{-1}
$k_{12} = 0.10$ min^{-1}
$k_{32} = 0.04$ min^{-1}

Rat with liver fibrosis
$k_{21} = 1.53$ min^{-1}
$k_{12} = 0.29$ min^{-1}
$k_{32} = 0.03$ min^{-1}

Fig. 4 Box plots of pharmacokinetic parameters (**A**, k_{21}; **B**, k_{32} and **C**, k_{12}) in control rats and rats with advanced fibrosis. The influx and efflux rates k_{21} and k_{32} are significantly decreased in rats with advanced liver fibrosis relative to those in control rats, whereas the backflux k_{12} is significantly increased. Lines in boxes represent medians, lower and upper limits of boxes represent 25th and 75th percentiles, and whiskers represent 10th and 90th percentiles. Outliers are shown as individual points

transporter Mrp2, and an increase in Mrp3, a sinusoidal backflux transporter of gadoxetate [4]. The diminished number of hepatocytes in advanced fibrosis might also partially explain the decrease in k_{21} and k_3, but not the increase in k_{12}.

With compartmental modelling, we thus showed here that the changes in hepatocyte transporter expression in liver fibrosis have a synergistic role in shifting the bidirectional hepatic transport route for gadoxetate from the hepatobiliary direction toward the hepatosinusoidal direction via Mrp3, which is up-regulated. This shift in gadoxetate transport has also been suggested previously in congenital deficiency of Mrp2 expression [6]. The combined changes in hepatocyte rates underscore the importance of the backflux transport pathway in hepatic clearance [23, 24].

It should be noted that k_{12} was larger than k_{32} in our study. These results differ from those obtained with ^{99m}Tc-IDA in patients by Araikum et al. [8]. Indeed, mean k_{12} was smaller than mean k_{32} in the Araikum study. These differences might be explained by species differences, but the fact that we neglected k_{01} might also have artificially increased k_{12}. Therefore, the rate constant values in our study should be regarded as relative rather than absolute measurements.

However, our findings that the backflux measured with gadoxetate-enhanced MR imaging increased and the biliary efflux decreased in advanced fibrosis remain valid.

Several studies have suggested using dynamic gadoxetate-enhanced MR imaging to obtain biomarkers of hepatic function in liver fibrosis [10–14]. However, these studies were limited by the fact that only hepatic uptake extraction was calculated. Here, we show that a complete description of hepatic transport dysfunction in hepatic fibrosis can be obtained with a bidirectional hepatocyte compartmental model. Indeed, this model not only allows calculation of the hepatocyte influx, but also the efflux and backflux, reflecting the true intrinsic hepatic clearance capacity [9]. Assessing liver function with gadoxetate-enhanced MR imaging in patients with liver fibrosis or cirrhosis may be useful not only to predict disease prognosis, but also to evaluate the efficacy and toxicity of drugs using the hepatic anion transporter system [6, 9]. In contrast to the dynamic MR imaging method developed here, static MR signal intensity measurements during the hepatobiliary phase after gadoxetic acid injection have been proposed to assess enhancement ratios or changes in T1 relaxation times between pre- and post-contrast images as
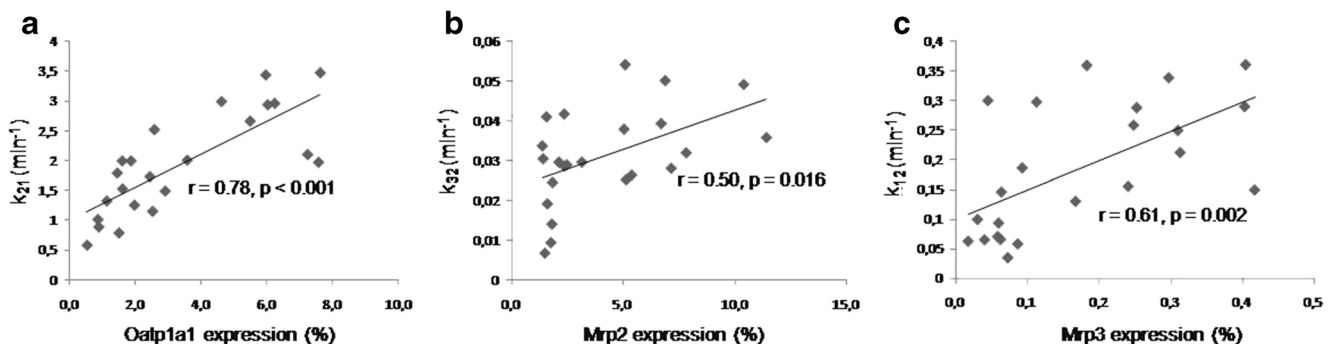
Fig. 5 Graphs showing significant correlations between hepatocyte influx rate k_{21} and hepatocyte transporter Oatp1a1 expression (**A**), biliary efflux rate k_{32} and Mrp2 (**B**), and sinusoidal backflux rate k_{12} and Mrp3 (**C**)

indicators of fibrosis or liver function [25–27]. However, these static methods do not allow precise measurement of the changes in membrane transport function during chronic liver diseases.

Some limitations of our study should be taken into account. First, deconvolution is sensitive to noise and even if we increased the signal-to-noise ratio by averaging our data and using a truncated singular value decomposition, oscillations remained in the liver impulse curve after deconvolution and were a limiting factor for the accuracy of the fitted parameters. Combining the dual-input one-compartmental Materne–Van Beers perfusion model [28] with the current three-compartmental hepatocyte model would be an alternative approach without the need for deconvolution. However, with this complete dual-input three-compartmental hepatobiliary model, eight parameters (arterial and portal venous flows, transit times (time delays) between arterial or portal venous and liver ROIs, hepatic venous outflow rate, and hepatocyte influx, efflux and backflux rates) would have to be fitted. This high number of variables may potentially lead to aberrant solutions, non-convergence and local minima. In particular, the results may be particularly sensitive to the arterial and portal venous time delays [29].

Second, the vascular ROIs in our study were segmented manually, which could lead to significant variability. Automatic or semiautomatic segmentation [30, 31] might be a beneficial way of decreasing this variability, although a good correlation between manual and automatic iliac arterial input functions was observed in Sanz-Requena et al. [30].

Third, we used saturation bands above and beneath the liver sections to avoid inflow effects. The drawback of this method is related to the fact that if may affect the signal concentration relationship in blood and stationary tissue differently. This again underscores the fact that rate constants in our study should be considered as relative values. An alternative to the use of saturation bands would be the use of non-slice-selective 90° or 180° preparation pulses and spoiler gradients [19].

Fourth, we did not take the differences in relaxivity of gadoxetate between blood and hepatocytes into account. It should be noted that the relaxivity of gadoxetate was reported to be 11.2 L/mmol · s in blood and 16.6 L/mmol · s in the liver at 0.47 T [32]. However, the relaxivities are known to decrease at increasing field strength. Shen et al. have recently reported that the r_1 relaxivity of gadoxetate are 7.2 L/mmol · s at 1.5 T and 4.9 L/mmol · s at 7 T [33]. The corresponding relaxivities in liver have not been reported, but the differences in relaxivity between blood and liver are also expected to decrease at higher field strengths. This is suggested by the results of Rohrer et al. showing that the differences in relaxivity between several contrast agents related to their protein binding decrease at increasing field strength [34].

Fifth, because in our experimental protocol fibrosis was induced by CCl4 injections for 8 or 12 weeks, only rats with advanced liver fibrosis were included in the study. It remains to be shown in future studies if compartmental modelling of gadoxetate transport is also useful to stage less advanced (F1 – F2) fibrosis.

It is concluded that the changes in hepatic anion transport function in rats with advanced liver fibrosis, namely decreased hepatocyte influx and biliary efflux, as well as increased sinusoidal backflux, can be assessed with a three-compartmental hepatocyte model at gadoxetate-enhanced MR imaging.

These kinetic parameters, which reflect the hepatic bidirectional transport function and are correlated with hepatocyte transporter expression, are potential predictive and prognostic biomarkers in liver fibrosis and cirrhosis.

Appendix

By assuming linear tracer kinetics to describe uptake and elimination of gadoxetate in hepatocytes [12], kinetic indexes can be derived by the linear system theory such as:

$$\frac{dx^j(t)}{dt} = A_{ji}x^i(t) + B_{ji}u^i(t) \tag{1.1}$$

The $x^i(t)$, j, i = 1…n with n the number of compartments, describe the time t evolution of gadoxetate in each compartment. A_{ji} is the flow into and out of each compartment, $u^i(t)$ are the input control functions for each compartment and B_{ji} the matrix describing the method of control application. By integrating Eq. 1.3 with $x^i(0) = 0$ for all i as initial conditions:

$$x^j(t) = e^{Ajit}x^i(0) + \int_0^t d\tau e^{Aji(t-\tau)}B_{ji}u^i(\tau) \tag{1.2}$$

Here, h(t) can be decomposed as the sum of the evolution of the gadotexate concentration into two compartments (hepatocytes and intra-hepatic bile ducts):

$$h(t) = x^1(t) + x^2(t) \tag{1.3}$$

$$h(t) = k_{21} \int_0^t d\tau \left[e^{-(k_{32}+k_{12})t}(t-\tau) + \left(\frac{k_{32}}{k_{32} + k_{12}-k_3} \left(e^{-k_3 t} - e^{-(k_{32}+k_{12})t} \right) \right)(t-\tau) \right] B(\tau) \tag{1.4}$$

$$h(t) = k_{21} \int_0^t d\tau \left[e^{-(k_{32}+k_{12})t}(t-\tau) + \left(\frac{k_{32}}{k_{32} + k_{12}-k_3} \left(e^{-k_3 t} - e^{-(k_{32}+k_{12})t} \right) \right)(t-\tau) \right] \tag{1.5}$$

$$h(t) = k_{21} - \frac{k_{21}k_{32}}{k_{32} + k_{12}-k_3} e^{-(k_{32}+k_{12})t} + \frac{k_{21}k_{32}}{k_{32} + k_{12}-k_3} e^{-k_3 t} \tag{1.6}$$

References

1. International Transporter Consortium, Giacomini KM, Huang SM et al (2010) Membrane transporters in drugdevelopment. Nat Rev Drug Discov 9:215–236

2. Stieger B, Heger M, de Graaf W, Paumgartner G, van Gulik T (2012) The emerging role of transport systems in liver function tests. Eur J Pharmacol 675:1–5

3. Roth M, Obaidat A, Hagenbuch B (2012) OATPs, OATs and OCTs: the organic anion and cation transporters of the SLCO and SLC22A gene superfamilies. Br J Pharmacol 165:1260–1287

4. Gu X, Manautou JE (2012) Regulation of hepatic ABCC transporters by xenobiotics and in disease states. Drug Metab Rev 42:482–538

5. Van Beers BE, Pastor CM, Hussain HK (2012) Primovist, Eovist: what to expect? J Hepatol 57:421–429

6. Jia J, Puls D, Oswald S et al (2014) Characterization of the intestinal and hepatic uptake/efflux transport of the magnetic resonance imaging contrast agent gadolinium-ethoxylbenzyl-diethylenetriamine-pentaacetic acid. Investig Radiol 49:78–86

7. Gambhir SS, Hawkins RA, Huang SC, Hall TR, Busuttil RW, Phelps ME (1989) Tracer kinetic modeling approaches for the quantification of hepatic function with technetium-99m DISIDA and scintigraphy. J Nucl Med 30:1507–1518

8. Araikum S, Mdaka T, Esser JD, Zuckerman M (1996) Hepatobiliary kinetics of technetium-99m-IDA analogs: quantification by linear systems theory. J Nucl Med 37:1323–1330

9. Peters AM (1998) Fundamental of tracer kinetics for radiologists. Br J Radiol 71:1116–1129

10. Nilsson H, Nordell A, Vargas R, Douglas L, Jonas E, Blomqvist L (2009) Assessment of hepatic extraction fraction and input relative blood flow using dynamic hepatocyte-specific contrast-enhanced MRI. J Magn Reson Imaging 29:1323–1331

11. Sourbron S, Sommer WH, Reiser MF, Zech CJ (2012) Combined quantification of liver perfusion and function with dynamic gadoxetic acid-enhanced MR imaging. Radiology 263:874–883

12. Nilsson H, Blomqvist L, Douglas L, Nordell A, Jonas E (2010) Assessment of liver function in primary biliary cirrhosis using Gd-EOB-DTPA-enhanced liver MRI. HPB 12:567–576

13. Nilsson H, Blomqvist L, Douglas L et al (2013) Gd-EOB-DTPA-enhanced MRI for the assessment of liver function and volume in liver cirrhosis. Br J Radiol 86:20120653

14. Lagadec M, Doblas S, Giraudeau C et al (2015) Advanced fibrosis: correlation between pharmacokinetic parameters at dynamic gadoxetate-enhanced MR imaging and hepatocyte organic anion transporter expression in rat liver. Radiology 274:379–386

15. Haimerl M, Schlabeck M, Verloh N et al (2016) Volume-assisted estimation of liver function based on Gd-EOB-DTPA-enhanced MR relaxometry. Eur Radiol 26:1125–1133

16. Starkel P, Leclercq IA (2011) Animal models for the study of hepatic fibrosis. Best Pract Res Clin Gastroenterol 25:319–333

17. Rusinek H, Lee VS, Johnson G (2001) Optimal dose of Gd-DTPA in dynamic MR studies. Magn Reson Med 46:312–316

18. Braet F, Wisse E (2002) Structural and functional aspects of liver sinusoidal endothelial cell fenestrae: a review. Comp Hepatol 1:1–17

19. Van Beers BE, Materne R, Annet L et al (2003) Capillarization of the sinusoids in liver fibrosis: noninvasive assessment with contrast-enhanced MRI in the rabbit. Magn Reson Med 49:692–699

20. Veteläinen RL, Bennink RJ, de Bruin K, van Vliet A, van Gulik TM (2006) Hepatobiliary function assessed by 99mTc-mebrofenin cholescintigraphy in the evaluation of severity of steatosis in a rat model. Eur J Nucl Med Mol Imaging 33:1107–1114

21. Blouin A, Bolender RP, Weibel ER (1977) Distribution of organelles and membranes between hepatocytes and non hepatocytes in the rat liver parenchyma. A stereological study. J Cell Biol 72:441–455

22. Bedossa P (1994) Intraobserver and interobserver variations in liver biopsy interpretation in patients with chronic hepatitis C. Hepatology 20:15–20

23. Peters AM, Myers MJ, Mohammadtaghi S, Mubashar M, Mathie RT (1998) Bidirectional transport of iminodiacetic organic anion analogues between plasma and hepatocyte. Eur J Nucl Med 25:766–773

24. Pfeifer ND, Hardwick RN, Brouwer KL (2014) Role of hepatic efflux transporters in regulating systemic and hepatocyte exposure to xenobiotics. Annu Rev Pharmacol Toxicol 54:509–535

25. Yoon JH, Lee JM, Paek M, Han JK, Choi BI (2016) Quantitative assessment of hepatic function: modified look-locker inversion recovery (MOLLI) sequence for T1 mapping on Gd-EOB-DTPA-enhanced liver MR imaging. Eur Radiol 26:1775–1782

26. Geisel D, Lüdemann L, Fröling V et al (2015) Imaging-based evaluation of liver function: comparison of 99mTc-mebrofenin hepatobiliary scintigraphy and Gd-EOB-DTPA-enhanced. MRI. Eur Radiol 25:1384–1391

27. Ba-Ssalamah A, Bastatai N, Wibmer A et al (2016) Hepatic gadoxetic acid uptake as a measure of liver disease: where are we? J Magn Reson Imaging, in press

28. Materne R, Van Beers BE, Smith AM et al (2000) Non-invasive quantification of liver perfusion with dynamic computed tomography and a dual-input one-compartmental model. Clin Sci 99:517–525

29. Kershaw LE, Buckley DL (2006) Precision in measurements of perfusion and microvascular permeability with T1-weighted dynamic contrast-enhanced MRI. Magn Reson Med 56:986–992

30. Sanz-Requena R, Prats-Montalbán JM, Martí-Bonmatí L (2015) Automatic individual arterial input functions calculated from PCA outperform manual and population-averaged approaches for the pharmacokinetic modeling of DCE-MR images. J Magn Reson Imaging 42:477–487

31. Heye T, Merkle EM, Reiner CS et al (2013) Reproducibility of dynamic contrast-enhanced MR imaging. Part II. Comparison of intra- and interobserver variability with manual region of interest placement versus semiautomatic lesion segmentation and histogram analysis. Radiology 266:812–821

32. Schuhmann-Giampieri G, Schmitt-Willich H, Press WR, Negishi C, Weinmann HJ, Speck U (1992) Preclinical evaluation of Gd-EOB-DTPA as a contrast agent in MR imaging of the hepatobiliary system. Radiology 183:59–64

33. Shen Y, Goerner FL, Snyder C et al (2015) T1 relaxivities of gadolinium-based magnetic resonance contrast agents in human whole blood at 1.5, 3, and 7 T. Investig Radiol 50:330–338

34. Rohrer M, Bauer H, Mintorovitch J, Requardt M, Weinmann HJ (2005) Comparison of magnetic properties of MRI contrast media solutions at different magnetic field strengths. Investig Radiol 40:715–724h